ELSEVIER

Physica D 89 (1995) 123–135

PHYSICA D

Stability of cylindrical bodies in the theory of surface diffusion

Bernard D. Coleman, Richard S. Falk, Maher Moakher

Department of Mechanics and Materials Science and Department of Mathematics, Rutgers University, Piscataway, NJ 08855-0909, USA

Received 18 October 1994; revised 27 January 1995; accepted 27 January 1995
Communicated by J.M. Ball

Abstract

Perturbation arguments and finite element calculations are employed to study the nonlinear partial differential equations governing morphological changes induced by curvature-driven diffusion of mass in the surface of an axially symmetric body. Isotropy of surface properties is assumed. Second- and higher-order perturbation analyses indicate that the familiar result of the linear theory of small amplitude longitudinal perturbations of a cylinder to the effect that a long cylinder is stable against all perturbations with spatial Fourier spectra containing only wavelengths less than the circumference of the cylinder does not hold in the full nonlinear theory. The perturbation analyses yield criteria for determining when longitudinal perturbations with high wave-number spectra grow in amplitude, after an initial decay followed by an incubation time, and result in break-up of the body into a necklace of beads. The principal conclusions of the formal perturbation analyses are found to be in good accord with numerical solutions obtained by finite element methods.

PASC: 68.35.Fx
Keywords: Surface diffusion; stability of solids

1. Introduction

We are concerned here with the changes of shape induced in a materially isotropic and homogeneous solid body B by mass diffusion within the body's bounding surface S. Following Herring [1] and Mullins [2], we employ the constitutive equation,

$$\boldsymbol{q} = -K \nabla_S H \,. \tag{1}$$

to relate the mass flux $\boldsymbol{q}$ in S to the gradient in S of the sum H of the principal curvatures of S. The positive material constant K is proportional to the surface self-diffusion coefficient of the material of which B is composed. When, as we assume here, there is no motion other than the flux of mass $\boldsymbol{q}$, balance of mass implies that the rate v of advance of S along its exterior normal is related as follows to the surface divergence of $\boldsymbol{q}$ and the constant density ρ [2]:

$$\rho v + \operatorname{div}_S \boldsymbol{q} = 0 \,. \tag{2}$$

We here assume that the surface $S = S(t)$ is axially symmetric at each time t. To describe the evolution of S, we employ a cylindrical coordinate system with axis along the axis of symmetry and express the radial coordinate r of a point on S as a time-dependent function of the axial

SSDI 0167-2789(95)00261-8

coordinate x: $r = r(x, t)$. We regard the shape of S at $t = 0$ as a perturbation of a circular cylinder of radius a and write $r(x, 0) = r_0(x) = a[1 + \varepsilon u(x)]$.

In the axially symmetric case, Eqs. (1) and (2) yield a fourth-order partial differential equation for $r = r(x, t)$, which, after a change of units equivalent to replacement of t by $a^4\rho t/K$, r by ar, and x by ax, can be written

$$r_t = \frac{1}{r}\left[\frac{r}{[1 + (r_x)^2]^{1/2}} \times \left(\frac{1}{r[1 + (r_x)^2]^{1/2}} - \frac{r_{xx}}{[1 + (r_x)^2]^{3/2}}\right)_x\right]_x , \quad (3)$$

where $r_t, r_x, \ldots$ stand for $\partial r/\partial t$, $\partial r/\partial x, \ldots$. In the same dimensionless units, the initial condition for Eq. (3) is

$$r(x, 0) = r_0(x) = 1 + \varepsilon u(x) ; \quad (4)$$

$u(x)$ is assumed to be given for all x, and $\varepsilon > 0$ is such that $\varepsilon u(x) > -1$. In this paper we discuss cases in which u is an almost periodic function. The emphasis is laid on functions u that have a finite Fourier spectrum and hence can be taken to be of the form,

$$u(x) = \sum_{i=1}^{N} c_i \sin\left(\frac{2\pi}{P_i}x + \varphi_i\right) , \quad (5)$$

with c_i, $P_i > 0$.

Linearization of Eq. (3) about the state $r \equiv 1$ yields the equation,

$$r_t + r_{xx} + r_{xxxx} = 0 , \quad (6)$$

which, since the work of Nichols and Mullins [3], often has been used in the theory of surface diffusion to investigate the stability of cylinders against longitudinal perturbations.

The solution of the linear partial differential equation (6) with $r(x, 0)$ as in Eqs. (4) and (5) is

$$r(x, t) = 1 + \varepsilon w^{(1)}(x, t) , \quad (7)$$

where

$$w^{(1)}(x, t) = \sum_{i=1}^{N} c_i \, e^{\alpha(k_i)t} \sin(k_i x + \varphi_i) , \quad (8)$$

with

$$k_i = 2\pi/P_i > 0 \quad (9)$$

and (cf., Eq. (4) of [3])

$$\alpha(k) = k^2[1 - k^2] . \quad (10)$$

A graph of α versus k is shown in Fig. 1. The maximum value of $\alpha(k)$ is 1/4 and occurs at $k = 2^{-1/2}$. As $\alpha(k_i) > 0$ only for $k_i < 1$, the linear theory yields exponential decay of the initial perturbation whenever $P_i < 2\pi$ for all i, i.e., whenever each period P_i in Eq. (5) is less than the circumference of the unperturbed cylinder. In this paper we show that this conclusion does not hold for the full nonlinear partial differential equation (3).

We give here a perturbation analysis and numerical calculations implying, among other things, that when $P_i < 2\pi$ for all i, although the solution of Eq. (3) shows, *for small t*, a decay of the sinusoidal perturbations described by Eqs. (4) and (5), if $N \geq 2$ and if at least two distinct numbers P_i, P_j in Eq. (5) are sufficiently close that $|P_i^{-1} - P_j^{-1}|^{-1} > 2\pi$, i.e., are such that $|k_i - k_j| < 1$, then, after an incubation time whose duration can be estimated, new sinusoidal terms with wavelength greater than 2π appear in the solution of Eq. (3). These new sinusoidal terms grow in amplitude, and the surface eventually departs far from cylindrical shape in a process

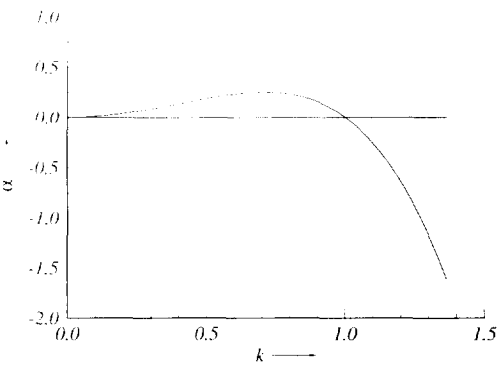

Fig. 1. The rate of growth α as a function of the wave number k according to the dispersion relation (10).

that, according to the numerical results reported in Section 5, results in a finite time in break-up of the body into separated subbodies. As we observe in Sections 4 and 5, when $P_i < 2\pi$, i.e., $k_i > 1$, for all i, even if there is not a pair (i, j) with $0 < |k_i - k_j| < 1$, it can happen that, again after an incubation time, new sinusoidal terms appear in the solution and grow, resulting in break-up; a sufficient condition for this is that the additive group generated by the numbers $k_i = 2\pi/P_i$, with P_i as in Eq. (5), contain a positive term less than 1, i.e., that there be integers m_i, positive, negative, or zero, such that $0 < \sum_{i=1}^{N} m_i k_i < 1$.

2. General properties of diffusion in axially symmetric surfaces

For the remainder of the paper we employ for r, x, and t the dimensionless units of Eqs. (3) and (4). In these units, for an axially symmetric body, Eqs. (1) and (2) become

$$q = -H_x[1 + (r_x)^2]^{-1/2}, \tag{11}$$

$$rr_t = -(rq)_x, \tag{12}$$

where

$$rH = [1 + (r_x)^2]^{1/2} - (rr_x[1 + (r_x)^2]^{-1/2})_x. \tag{13}$$

To clarify the significance of Eq. (11) we note that for a scalar-valued function h of x and t, such as H or r, $h_x[1 + (r_x)^2]^{-1/2} = |\nabla_S h|\mathrm{sign}(h_x)$, which is the derivative at time t of h with respect to arclength along the curve defined in an (x, y)-plane by the function $y = r(x, t)$; if we write $\boldsymbol{t}$ for the unit vector tangent to this curve, then $\boldsymbol{q} = q\boldsymbol{t}$. Elimination of q from Eqs. (11) and (12) yields Eq. (3).

The volume and surface area of the portion of B between the planes $x = X_1$ and $x = X_2$ are

$$V(t; X_1, X_2) = \pi \int_{X_1}^{X_2} r^2 \, dx, \tag{14}$$

$$\Psi(t; X_1, X_2) = 2\pi \int_{X_1}^{X_2} r[1 + (r_x)^2]^{1/2} \, dx. \tag{15}$$

The surface area $\Psi(t; X_1, X_2)$, or, more precisely, the product of this area with the surface tension, may be identified with the Helmholtz free energy of the indicated portion of B. When $r(x, t)$ obeys Eq. (3), we have

$$\frac{\partial}{\partial t} V(t; X_1, X_2) = 2\pi[rH_x[1 + (r_x)^2]^{-1/2}]_{X_1}^{X_2}, \tag{16}$$

$$\frac{\partial}{\partial t} \Psi(t; X_1, X_2) = -2\pi \int_{X_1}^{X_2} \frac{r(H_x)^2}{[1 + (r_x)^2]^{1/2}} \, dx + 2\pi \left[\frac{r[r_x r_t + HH_x]}{[1 + (r_x)^2]^{1/2}} \right]_{X_1}^{X_2}. \tag{17}$$

For a solution of Eq. (3) on $(\infty, \infty) \times [0, T)$ with spatial period P, or, equivalently, a solution on $[0, P] \times [0, T)$ obeying the boundary conditions,

$$r(0, t) = r(P, t), \quad H(0, t) = H(P, t), \tag{18a}$$

$$r_x(0, t) = r_x(P, t), \quad H_x(0, t) = H_x(P, t), \tag{18b}$$

we write $V(t, P)$, $\Psi(t, P)$ for $V(t; 0, P)$, $\Psi(t; 0, P)$, and note that (16) and (17) yield

$$\frac{\partial}{\partial t} V(t, P) = 0, \tag{19}$$

$$\frac{\partial}{\partial t} \Psi(t, P) = -2\pi \int_0^P \frac{r(H_x)^2}{[1 + (r_x)^2]^{1/2}} \, dx = -2\pi \int_0^P rq^2[1 + (r_x)^2]^{1/2} \, dx \leq 0. \tag{20}$$

Thus, for such solutions the volume $V(t, P)$ is preserved and the surface area $\Psi(t, P)$ is a Lyapunov function that is strictly decreasing when the total curvature H is not constant in x, i.e., when q in Eq. (11) is not zero for all x.

When u in Eq. (4) and the corresponding solution r of Eq. (3) are almost periodic in x, but not necessarily periodic, the average volume,

$$\langle v \rangle = \lim_{X \to \infty} V(t; -X, X)/2X, \tag{21}$$

is independent of t, and the average area,

$$\langle \psi \rangle(t) = \lim_{X \to \infty} \Psi(t; -X, X)/2X , \tag{22}$$

is monotone decreasing in t for $t \geq 0$. When Eq. (5) holds,

$$\langle v \rangle = \pi \left[1 + \tfrac{1}{2} \varepsilon^2 \sum_{i=1}^{N} c_i^2 \right] . \tag{23}$$

When the numbers P_i in Eq. (5) are rationally related, r is periodic with a period P that can be taken to be any common integral multiple of all the P_i, and then $\langle v \rangle = V(t, P)/P$, $\langle \psi \rangle(t) = \Psi(t, P)/P$.

Let r_* be given by

$$\pi r_*^2 = \langle v \rangle . \tag{24}$$

The number r_* is in general not the radius a of the unperturbed cylinder (which equals 1 in the present units). In the case in which u obeys Eq. (5), r_* differs from a by terms $\mathcal{O}(\varepsilon^2)$. In the next section we employ the methods of perturbation theory to study the behaviour of the quantity,

$$g(t) = \sup_x |r(x, t) - r_*| , \tag{25}$$

measuring the departure, at time t, of the body from cylindrical shape.

3. Second-order perturbation analysis

When the function u in Eq. (5) is specified and held fixed, r depends on ε; we suppose that this dependence is sufficiently smooth that we can write, for all x and for t in a set of the form $[0, T)$,

$$r(x, t; \varepsilon) = 1 + \varepsilon w^{(1)}(x, t) + \varepsilon^2 w^{(2)}(x, t) + \mathcal{O}(\varepsilon^3) . \tag{26}$$

By placing this expression in Eq. (3) and equating the coefficients of equal powers of ε on the two sides of that equation, we obtain

$$w_t^{(1)} + (w_{xx}^{(1)} + w^{(1)})_{xx} = 0 , \tag{27}$$

$$w_t^{(2)} + (w_{xx}^{(2)} + w^{(2)})_{xx} = (w_x^{(1)})^2 + 2w^{(1)} w_{xx}^{(1)} - (w_{xx}^{(1)})^2 - 2w_x^{(1)} w_{xxx}^{(1)} . \tag{28}$$

It follows from Eqs. (4) and (26) that

$$w^{(1)}(x, 0) = u(x) , \tag{29}$$

$$w^{(2)}(x, 0) = 0 . \tag{30}$$

Solution of Eq. (27) with the initial condition (29) yields the function $w^{(1)}$, and once $w^{(1)}$ is known, (28) and (30) determine $w^{(2)}$.

The linear theory of small perturbations of a cylinder, which employs Eq. (6), is obtained by neglecting terms $\mathcal{O}(\varepsilon^2)$ in Eq. (26) and hence rests on Eqs. (27), (29), and the approximate relation (7). When $u(x)$ is as in Eq. (5), the solution of Eqs. (27) and (29) is that shown in Eqs. (8)–(10).

To evaluate the term $\mathcal{O}(\varepsilon^2)$ in Eq. (26), we place (8) in (28), employ (30), and obtain, after some calculation,

$$w^{(2)}(x, t) = A_0(t) + \sum_{i=1}^{N} A_1(i; t) \cos(2k_i x + 2\varphi_i) + \sum_{1 \leq i < j \leq N} [A_2(i, j; t) \cos((k_i + k_j)x + \varphi_i + \varphi_j) + A_3(i, j; t) \cos((k_i - k_j)x + \varphi_i - \varphi_j)] , \tag{31}$$

where

$$A_0(t) = \tfrac{1}{4} \sum_{i=1}^{N} c_i^2 [1 - e^{2\alpha(k_i)t}] , \tag{32a}$$

$$A_1(i; t) = \frac{3}{2} \frac{c_i^2 \beta(k_i)}{2\alpha(k_i) - \alpha(2k_i)} \times [e^{2\alpha(k_i)t} - e^{\alpha(2k_i)t}] , \tag{32b}$$

$$A_2(i, j; t) = \frac{c_i c_j \beta^+(k_i, k_j)}{\alpha(k_i) + \alpha(k_j) - \alpha(k_i + k_j)} \times [e^{[\alpha(k_i) + \alpha(k_j)]t} - e^{\alpha(k_i + k_j)t}] , \tag{32c}$$

$$A_3(i, j; t) = \frac{c_i c_j \beta^-(k_i, k_j)}{\alpha(k_i) + \alpha(k_j) - \alpha(k_i - k_j)} \times [e^{[\alpha(k_i) + \alpha(k_j)]t} - e^{\alpha(k_i - k_j)t}] , \tag{32d}$$

with α as in Eq. (10), k_i as in Eq. (9), and

$$\beta(k) = k^2[1 + k^2] , \tag{33a}$$

$$\beta^+(k_i, k_j) = [k_i k_j + k_i^2 + k_j^2][1 + k_i k_j]\,, \tag{33b}$$

$$\beta^-(k_i, k_j) = [k_i k_j - k_i^2 - k_j^2][1 - k_i k_j]\,. \tag{33c}$$

When $k_i > 1$ for each i, the quantities $\alpha(k_i)$, $\alpha(2k_i)$, $\alpha(k_i + k_j)$ are negative for each i and $j > i$, and hence not only $w^{(1)}$ but also all the terms in $w^{(2)}$, other than the constant term, $\frac{1}{4}\Sigma_i c_i^2$, and possibly some of the form $f(k_i, k_j; t)\cos((k_i - k_j)x + \varphi_i - \varphi_j)$ with

$$f(k_i, k_j; t) = \frac{c_i c_j \beta^-(k_i, k_j)}{\alpha(k_i - k_j) - \alpha(k_i) - \alpha(k_j)} \times e^{\alpha(k_i - k_j)t}\,, \tag{34}$$

will decay to zero exponentially with increasing t. The coefficient $|f(k_i, k_j; t)|$ of $\cos((k_i - k_j)x + \varphi_i - \varphi_j)$ is constant if $|k_i - k_j| = 1$; it grows exponentially in time if and only if

$$0 < |k_i - k_j| < 1\,. \tag{35}$$

The period $P_{i,j}$ of the envelope of the sum of two terms $c_i \sin(2\pi/P_i\, x + \varphi_i)$, $c_j \sin(2\pi/P_j\, x + \varphi_j)$ in Eq. (5) with $P_j > P_i$ is given by

$$P_{i,j}^{-1} = P_i^{-1} - P_j^{-1}\,. \tag{36}$$

The condition (35) for (exponential) growth of $|f(k_i, k_j; t)|$ is equivalent to the inequality

$$P_{i,j} > 2\pi\,. \tag{37}$$

In other words, if one takes ε in Eq. (4) to be sufficiently small that for short times the terms $\mathcal{O}(\varepsilon^2)$ in Eq. (26) can be neglected, then provided each period P_i in Eq. (5) is less than the circumference, 2π, of the unperturbed cylinder, and there is at least one pair (i, j) for which the period of the envelope of the corresponding two terms in Eq. (5) exceeds 2π, then for short times $r(x, t)$ will be well approximated by the expression

$$1 + \varepsilon^2 \cdot \tfrac{1}{4} \sum_{i=1}^{N} c_i^2 + \varepsilon \sum_{i=1}^{N} c_i\, e^{\alpha(k_i)t} \sin(k_i x + \varphi_i)\,, \tag{38}$$

where each $\alpha(k_i)$ is negative. Hence, after a brief time interval, $r(x, t)$ will be close, for all x, to the constant,

$$r_* = \left[1 + \tfrac{1}{2}\varepsilon^2 \sum_{i=1}^{N} c_i^2\right]^{1/2} = 1 + \varepsilon^2 \cdot \tfrac{1}{4} \sum_{i=1}^{N} c_i^2 + \mathcal{O}(\varepsilon^4)\,, \tag{39}$$

and the body will be nearly indistinguishable from a cylinder. In a subsequent time interval, however, $r(x, t)$ will be approximated by

$$1 + \varepsilon^2 \cdot \tfrac{1}{4} \sum_{i=1}^{N} c_i^2 + \varepsilon^2 \sum_{(i,j)\in\Gamma} f(k_i, k_j; t)\cos((k_i - k_j)x + \varphi_i - \varphi_j)\,, \tag{40}$$

where f is as in Eq. (34) and Γ is the set of pairs (i, j) with $1 \leq i < j \leq N$ and $0 < |k_i - k_j| < 1$; in that interval, $g(t)$, defined in Eq. (25), will increase.

Let ν be the minimum value that $g(t)$ must have for a departure of the body from cylindrical shape to be easily observable after $g(t)$ has decayed and started to increase. A reasonable value for ν would be, say, 0.05. The time $t_\#$ at which $g(t)$ attains the value ν after an initial decrease may be called the *incubation time* (for easily observable growth of a perturbation that, according to the linear equation (6), would only decay).

Our second-order perturbation analysis gives the following relation for $t_\#$ in the case in which there is precisely one pair (i, j) for which (35) holds:

$$\varepsilon^2 f(k_i, k_i; t_\#) = \nu\,. \tag{41}$$

This relation implies that $t_\#$ varies slowly, i.e., logarithmically, with ε. For large k, $\alpha(k)$ decreases with increasing k as $-k^4$. However, since, as we have noted, on the interval $0 < k < 1$ where $\alpha(k) > 0$, the maximum value of $\alpha(k)$ is only 1/4, $t_\#$ can be orders of magnitude longer than the time required for the initial decay of $g(t)$.

The first numerical experiment reported in Section 5 is a case in which $N = 2$ with $k_1 = 5$ and $k_2 = 11/2$ and hence the relation (35) holds with each $k_i > 1$. As we shall see, the growth in perturbations predicted by Eqs. (31)–(34) proceeds until there is a time t^* and values x^* of x for which $\lim_{t \to t^*-} r(x^*, t) = 0$. As a topological change occurs at $t = t^*$ that results in a transformation of the original infinitely long body into separated subbodies of finite length, we call t^* the "time of break-up".

4. Conclusions from higher-order analyses

Observations made in the previous section can be extended to a perturbation analysis of order n by replacing (26) with

$$r(x, t; \varepsilon) = 1 + \sum_{l=1}^{n} \varepsilon^l w^{(l)}(x, t) + \mathcal{O}(\varepsilon^{n+1}) \tag{42}$$

and keeping in Eq. (3) all terms of order ε^n. Among the results obtained in this way is the following important generalization of the conclusion about initial data with $k_i > 1$ for each i, but $0 < |k_i - k_j| < 1$ for a pair (i, j): If, in Eq. (5), $N \geq 2$ and

$$k_i > 1 \quad \text{for } i = 1, \ldots, N , \tag{43a}$$

but there is an integer $n \geq 2$ and N integers m_i that are positive, negative, or zero, such that

$$\sum_{i=1}^{N} |m_i| = n , \tag{43b}$$

$$0 < \sum_{i=1}^{N} m_i k_i < 1 , \tag{43c}$$

then, after an initial decay, the perturbation will grow as a sum of exponential terms, each of which is of the form,

$$C\, \mathrm{e}^{\alpha(k)t} \cos(kx + \varphi) , \tag{44a}$$

with C constant and

$$k = \sum_{i=1}^{N} m_i k_i , \quad \varphi = \tfrac{1}{2} n\pi + \sum_{i=1}^{N} m_i \varphi_i . \tag{44b}$$

The perturbation analysis that gives the above result yields also the conclusion that if for a given positive integer n it happens that, for *every* N-tuple $(m_1, \ldots, m_N)$ of integers m_i that are positive, negative, or zero and have $1 \leq \sum_{i=1}^{N} |m_i| \leq n$, there holds

$$\left| \sum_{i=1}^{N} m_i k_i \right| > 1 , \tag{45}$$

then expansions of order n and less in ε yield the conclusion that $g(t)$ decays to zero exponentially with increasing t.

The second numerical experiment described in Section 5 concerns a case in which $N = 3$, $k_i > 1$ for each i, and there is *no* pair (i, j) with $0 < |k_i - k_j| < 1$, but the wave numbers k_i are such that the relations (43a)–(43c) hold for $n = 3$ and an appropriate triplet (m_1, m_2, m_3). It there turns out that although a term entering in the analysis at order three in ε determines the early stages of the growth of the perturbation (after its initial decay), another term, entering at order five in ε, strongly influences the configuration of the body at later times.

The conclusions of the higher-order perturbation analysis for the case in which Eq. (5) holds suggest conjectures about solutions of Eq. (3) for a more general case in which u is an almost periodic function with a Fourier spectrum that is not necessarily finite.

To state the conjectures we recall some facts about almost periodic functions on the real line. For such functions the averages,

$$\eta(k) = \mathcal{M}\{u(x)\, \mathrm{e}^{-ikx}\} = \lim_{X \to \infty} \frac{1}{X} \int_{z}^{z+X} u(x)\, \mathrm{e}^{-ikx}\, \mathrm{d}x , \tag{46}$$

are finite-valued, independent of the choice of z, and vanish for all but a countable number of values k_j of k. For these values we may write the corresponding Fourier coefficients $\eta_j = \eta(k_j)$ in the form: $\eta_j = c_j\, \mathrm{e}^{i\psi_j}$, where $c_j = |\eta_j|$ is the amplitude associated with the wave number or

Fourier exponent k_j. It is customary to write (cf. [4, 5]):

$$u(x) \sim \sum_{j=1}^{\infty} \Re\, \eta_j\, e^{ik_j x} = \sum_{j=1}^{\infty} c_j \sin(k_j x + \varphi_j)\,, \qquad (47)$$

where $\varphi_j = \psi_j + \pi/2$. We remark in passing that the amplitudes c_j obey Parseval's equality:

$$\sum_{j=1}^{\infty} c_j^2 = \mathcal{M}\{u(x)^2\}\,. \qquad (48)$$

A set $\mathcal{A}$ of real numbers is said to form an additive group if for each pair (κ, λ) of numbers in $\mathcal{A}$ both $\kappa + \lambda$ and $\kappa - \lambda$ are in $\mathcal{A}$. We write Mod(u) for the smallest additive group of real numbers that contains all the Fourier exponents of u (cf. [5]). For our present purposes it is useful to define a number $\bar{\bar{k}} = \bar{\bar{k}}(u)$ by

$$\bar{\bar{k}} = \inf\{|\kappa|\,|\,\kappa \in \mathrm{Mod}(u),\, \kappa \neq 0\}\,. \qquad (49)$$

We have now assembled the apparatus needed to formulate the following two assertions about solutions of Eq. (3) for which u in Eq. (4) is a non-constant almost periodic function on $(-\infty, \infty)$:

Assertion 1. If

$$\bar{\bar{k}}(u) > 1\,, \qquad (50)$$

then, for ε sufficiently small, $g(t)$ decays to zero monotonically.

Assertion 2. Suppose that $\bar{\bar{k}}(u) < 1$, i.e., that Mod(u) contains at least one number κ with

$$0 < |\kappa| < 1\,. \qquad (51)$$

Then

(a) (*weak assertion*) $g(t)$ does not approach 0 as t increases,

(b) (*strong assertion*) break-up occurs in a finite time, i.e., there is a $t^* < \infty$ and points x^* with $\lim_{t \to t^*} r(x^*, t) = 0$.

These assertions are suggested by the perturbation analyses.

As regards the first assertion: If $\bar{\bar{k}}(u) > 1$, then, for each positive integer N, the inequality (45) holds for every N-tuple $(k_1, \ldots, k_N)$ of Fourier exponents k_i of u and every N-tuple $(m_1, \ldots, m_N)$ of integers m_i that are positive, negative, or zero; therefore, whenever the summation in Eq. (47) is replaced by a sum over a finite number of terms, for every positive integer n a perturbation analysis of order n yields the conclusion that $g(t)$ decays to zero exponentially with increasing t.

If the hypothesis of the second assertion is assumed, then the relation (51) holds with $\kappa = \sum_{i=1}^{N} m_i k_i$ (again with $(k_1, \ldots, k_N)$ a list of Fourier exponents of u and each m_i a positive, negative or zero integer). If one now defines n by Eq. (43b), then a perturbation analysis of order n, based on a replacement of the right-hand side of (47) by a sum over an arbitrarily large number of terms, provided those with the exponents $(k_1, \ldots, k_N)$ are included, yields the conclusion that, perhaps after an initial decay, $g(t)$ will grow exponentially.

Albeit we do not yet have rigorous proofs of the assertions, the observations just made and several numerical studies of the type reported below have convinced us of the correctness of Assertion 1 and the strong form of Assertion 2.

When u is P-periodic, Mod(u) is the set of all positive, negative, or zero integral multiples of $k = 2\pi/P$. Hence the first assertion implies that, as expected, if u is periodic with a period less than the circumference, 2π, of the unperturbed cylinder, then $g(t)$ decays to zero monotonically. If u is periodic with a period exceeding 2π, then, according to the second assertion (and our perturbation analyses) $g(t)$ does not approach 0, and, according to the strong form of the assertion, break-up occurs in a finite time.

For a quasiperiodic function u that is a sum of a finite number of periodic functions with periods $P_1, \ldots, P_i, \ldots, P_N$, Mod($u$) is just the additive group generated by the N numbers $k_i = 2\pi/P_i$, and hence, when such a function u is specified in Eq. (4), it is usually not difficult to deduce definite implications of the two asser-

tions; the exceptional cases are, of course, those in which $\bar{k}(u) = 1$.

5. Numerical solutions

We have developed a family of space–time finite element approximation schemes for obtaining numerical solutions of Eq. (3) on sets of the form $M = [0, P] \times [0, T)$ with the periodic boundary conditions seen in Eqs. (18) [6]. In the approximation schemes the analogue $\tilde{V}(t, P)$ of the total volume $V(t, P)$ is constant in time, i.e., is, in an exact sense, a conserved quantity, and the analogue $\tilde{\Psi}(t, P)$ of the surface area $\Psi(t, P)$ decreases in time and hence serves as a Lyapunov function.

Let us write

$$\Omega(x, t) = \tfrac{1}{2} r(x, t)^2 , \tag{52}$$

and observe that Eq. (13) can be written,

$$H = [2\Omega + (\Omega_x)^2]^{-1/2} - (\Omega_x [2\Omega + (\Omega_x)^2]^{-1/2})_x . \tag{53}$$

The approximation schemes employ a variational principle that rests upon the observation that each solution of Eq. (3) that obeys Eqs. (18) corresponds to a pair (Ω, H) of functions on M that obey the variational equations,

$$\langle \Omega_t \,|\, \zeta \rangle + \langle 2\Omega H_x (2\Omega + (\Omega_x)^2)^{-1/2} \,|\, \zeta_x \rangle = 0 , \tag{54a}$$

$$\langle H \,|\, \xi \rangle - \langle (2\Omega + (\Omega_x)^2)^{-1/2} \,|\, \xi \rangle - \langle \Omega_x (2\Omega + (\Omega_x)^2)^{-1/2} \,|\, \xi_x \rangle = 0 , \tag{54b}$$

for all sufficiently smooth test functions ζ, ξ on M with

$$\zeta(0, t) = \zeta(P, t) , \quad \xi(0, t) = \xi(P, t) . \tag{55}$$

The L^2-inner product of functions on $[0, P]$ is indicated here by the notation:

$$\langle Y \,|\, \xi \rangle = \int_0^P Y(x, t) \xi(x, t) \, dx . \tag{56}$$

In the numerical studies reported below, we have used initial data of the form seen in Eqs. (4) and (5) with the numbers P_i in Eq. (5) rationally related. The calculations were done with the simplest of the finite element schemes we have described in Ref. [6], namely that in which Ω is approximated by functions piecewise linear in x and t, and H is approximated by functions piecewise linear in x and piecewise constant in t.

For the first numerical experiment the initial data correspond to the function,

$$r_0(x) = 1 + 5 \times 10^{-2} [\sin(11x/2) + \sin(5x)] , \tag{57}$$

which has minimum period 4π and has $k_1 = 11/2 > 1$, $k_2 = 5 > 1$, $|k_1 - k_2| = 1/2 < 1$. According to the second-order perturbation analysis, the two sinusoidal terms with $k_i > 1$ should decay rapidly, and after this decay, which in the present case lasts until approximately $t = 2 \times 10^{-2}$, $r(x, t)$ should be, for a while, close to a cosine function of x which has period 4π and an amplitude growing as $e^{\alpha(1/2)t}$ with $\alpha(1/2) = 3/16$. For the finite element calculation the interval of x values was chosen to have length 8π, i.e., twice the minimum period of r_0, and was discretized into 512 equal segments. For the time interval $0 < t \leq 5 \times 10^{-2}$ that contains the times of rapid decay of $g(t)$, the time step, Δt, was chosen to be 10^{-4}; during the early growth phase, i.e., for $5 \times 10^{-2} < t \leq 28.05$, Δt was set equal to 10^{-2}; for $28.05 < t \leq 28.27234 = t^*$, the time steps were chosen so that Δt decreased rapidly as t approached t^*.

In Fig. 2 there are graphs of r versus x for several values of t. The initial data are shown in Fig. 2a. In Fig. 2b at $t = 10^{-2}$ remnants of the terms $5 \times 10^{-2} \sin(5x)$ and $5 \times 10^{-2} \sin(11x/2)$ can be seen perturbing the function $\tilde{r}(\cdot, t)$ given by

$$\tilde{r}(x, t) = r_* + \varepsilon^2 f(5, 11/2; t) \cos(x/2) \tag{58}$$

with $\varepsilon^2 = 2.5 \times 10^{-3}$ and f is as in (34). At $t = 1.63 \times 10^{-2}$, $g(t)$ attains its minimum value, and at that time the difference between $r(x, t)$

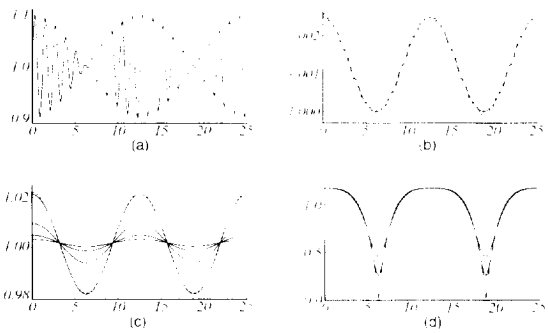

Fig. 2. The radius r as a function of x at various t for $r_0(x)$ as in Eq. (57): (a) $t = 0$; (b) $t = 10^{-2}$ (wavy line), $t = 1.63 \times 10^{-2}$; (c) $t = 0.1, 5, 10, 15$; the dashed curve gives the results of the second-order perturbation analysis at $t = 15$; (d) $t = 28$, 28.25, 28.27234.

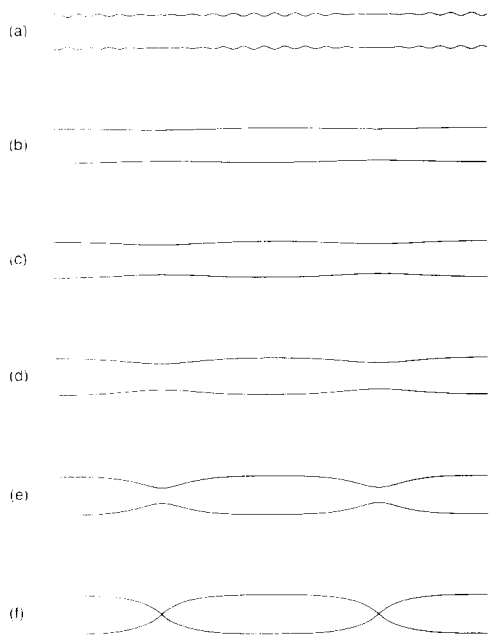

Fig. 3. Configurations attained at selected times before the break-up implied by the initial data of Eq. (57): (a) $t = 0$; (b) $t = 20$; (c) $t = 23$; (d) $t = 25.5$; (e) $t = 28$; (f) $t = t^* = 28.27234$.

and $\tilde{r}(x, t)$ is not detectable on the scale employed for r of Fig. 2b. Fig. 2c contains graphs for values of t at which $r(x, t)$ is close to $\tilde{r}(x, t)$. The earliest time at which the second-order perturbation analysis gives results, plotted with dashed curves, that are distinguishable from the finite element results, on the scale of Fig. 2c, is $t = 15$. Fig. 2d contains graphs of r versus t for t close to the time t^* of break-up. In the present case, $r(x^*, t^*) = 0$ at $x^* = 2\pi \pm 4\pi n$.

Fig. 3, which is drawn with equal scales for the ordinate and the abscissa, shows profiles of the axially symmetric body whose surface is given by $r = r(x, t)$. The initial configuration is seen in Fig. 3a. At a time $t \sim 10^{-2}$ the body is of cylindrical shape to within an error of the order 0.1% in r. If we set $\nu = 0.05$, then the finite-element results yield 19.55 for the incubation time, i.e., the first value, $t_\#$, of t at which $g(t)$ attains the value ν after $g(t)$ has decayed to its minimum value, and hence the configuration seen in Fig. 3b is that at the incubation time. In the present case the incubation time $t_\#$ accounts for about 69% of the time t^* required for the perturbed cylinder to evolve into the "necklace of beads" seen in Fig. 3f.

Table 1 contains for selected values of g the times t at which they are attained according to the finite-element calculations (t_F) and the second-order perturbation analysis (t_P). We note that here t_F and t_P agree to within 5% until $g \approx 0.2$.

The two numerical experiments we report here are cases in which the full nonlinear equation (3) yields a finite value for the time t^* of break-up, but the linear equation (6) yields decay of the perturbation without subsequent growth, and hence no break-up. (The one previous numerical study of nonlinear effects in the evolution of longitudinal perturbations of a cylinder of which we are aware is that of Marinis and Sekerka [7, 8] and is based on a finite difference scheme. For each numerical experiment they report, the

Table 1
Values of t at which specified values of g are obtained when r_0 is as in Eq. (57): t_F is obtained from the finite element calculation ; t_P from the second-order perturbation analysis

g	t_F	t_P	$(t_F - t_P)/t_F$
0.0500	19.55	19.72	0.009
0.1061	23.05	23.74	0.030
0.1959	25.55	27.81	0.050
0.5396	28.05	32.41	0.155

initial data are equivalent to a single sinusoidal term with $k < 1$ and hence the condition (43) does not hold, the linear theory yields a finite value for the time t^* of break-up, and the concept of an incubation time $t_\#$ does not arise, for there is no initial decay of the perturbation. In the cited work, Marinis and Sekerka give examples in which calculations are carried out up to time t^*, and it is reported that, as our analysis and calculations also indicate, Eq. (3) yields a smaller value of t^* than Eq. (6).) In general, linearization of Eq. (3) about the equilibrium state in which r is independent of x leads one to overestimate the time required for break-up or to miss the phenomenon completely.

The solution corresponding to Eq. (57) provides an example of a case in which the separated subbodies formed at time t^* remain star shaped with respect to a fixed point on the x-axis for all $t > t^*$, and hence the evolution of a subbody can be studied for $t > t^*$ by reparameterizing its surface with spherical coordinates. In the present case, the subbodies are congruent and for $t > t^*$ are star shaped with respect to the mid-points of successive values of x^*. The distance d from such a mid-point, x_0, to a point on the surface of the subbody containing x_0 was expressed as a function of t and the colatitude φ from the x-axis. Results obtained for $t > t^*$ employing a finite element program for $d(\varphi, t)$ analogous to that employed to calculate $r(x, t)$ for $t < t^*$ are shown in Fig. 4. The reader will note that when $\hat{t} = t - t^* = 0$, 10^{-3}, and 10^{-1}, the subbody is convex, and that this convexity, which is not present for $\hat{t} = 1$, returns before $\hat{t} = 4$. (Similar examples of such departure and return to convexity were given by Courtney and Lee [9] in their numerical study, with a finite difference scheme, of the cylinderization of plates by surface diffusion, a phenomenon that gives rise to problems with different symmetry than those we consider here. Experiments showing the phenomenon of cylinderization in a rolled nickel-tungsten alloy containing plate-like inclusions were reported by Malzahn Kampe, Courtney, and Leng [10].) In the theory of Eqs. (1) and (2), i.e., in the theory of *motion by Laplacian of mean curvature*, there is no analogue of Huisken's theorem [11] in the theory of *motion by mean curvature* to the effect that a surface convex at one time is convex at all later times.

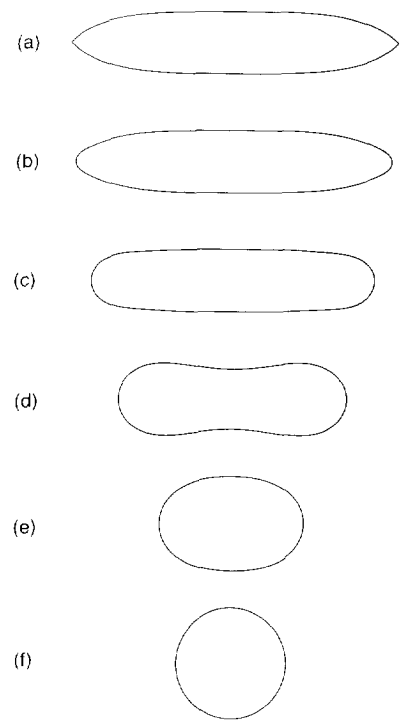

Fig. 4. Configurations attained at times $t = t^* + \hat{t}$ after the break-up implied by the initial data of Eq. (57): (a) $\hat{t} = 0$; (b) $\hat{t} = 10^{-3}$; (c) $\hat{t} = 10^{-1}$; (d) $\hat{t} = 1$; (e) $\hat{t} = 4$; (f) $\hat{t} = 10$.

The subbody configuration shown in Fig. 4 for $\hat{t} = 10$ is spherical in the sense that for it d is constant in φ to 6 figures. The set of spheres obtained in this way is the final equilibrium state of the original perturbed cylinder.

The initial data for the second numerical experiment correspond to the function

$$r_0(x) = 1 + 5 \times 10^{-2} \sum_{i=1}^{3} \sin(k_i x)\,,$$
$$k_1 = 21/5\,, \quad k_2 = 3\,, \quad k_3 = 3/2\,, \tag{59}$$

which has minimum period $20\pi/3$. In the present

case, not only is each k_i greater than 1, but, for $i \neq j$, $|k_i - k_j| > 1$. Hence first-order and second-order perturbation analyses both yield the conclusion that the perturbation should decay. However, as $k_3 + k_2 - k_1 = 3/10$, there is a triplet $\boldsymbol{m} = (m_1, m_2, m_3)$ such that (43b) and (43c) hold with $n = 3$. (In fact, $\boldsymbol{m}$ and $-\boldsymbol{m}$ with $\boldsymbol{m} = (-1, 1, 1)$ are the only such triplets). We may therefore conclude that a third-order analysis will show that the perturbation grows after its initial decay. In the early stages of this growth phase, r as a function of x is expected to show 2 turning points in the interval $0 \leq x < 20\pi/3$, although the initial data show 28 turning points in that interval. There are triplets $\boldsymbol{m}$ for which (43b) and (43c) hold with $n = 4$, e.g., $\boldsymbol{m} = (-1, 2, -1)$, but no such triplet yields an absolute value for the sum in (43c) other than 3/10. Among the triplets for which (43b) and (43c) hold with $n = 5$, there are some, e.g., $\boldsymbol{m} = (-2,3,0)$, which yield 6/10 for the absolute value of the sum in (43c). As

$$\alpha(0.6) = 0.2304 > \alpha(0.3) = 0.0819\,, \tag{60}$$

terms appearing in a fifth-order perturbation analysis with period $10\pi/3$ will influence the configuration at later times. When these terms become important, r as a function of x is expected to show 4 turning points in the interval $0 \leq x < 20\pi/3$.

For the finite element calculations employing Eq. (59), the interval $0 \leq x \leq 20\pi/3$, whose length equals the minimum period of r_0, was discretized into 512 equal segments; Δt was chosen to be 10^{-4} for the time interval $0 < t \leq 5 \times 10^{-2}$ that contains the times of rapid decay of the modes in the initial data with $k = 21/5$ and 3; for t in the interval $5 \times 10^{-2} < t \leq 64.78$, Δt was set equal to 10^{-2}; in the interval $64.78 < t \leq 64.7862 = t^*$, Δt was chosen so as to decrease rapidly as t^* is approached.

A graph of Eq. (59) is shown in Fig. 5a. In Figs. 5b–d, $g(t)$ increases as t increases. The minimum value of g is attained at a time close to $t = 12$, the earliest time for which r as a function of x is shown in Fig. 5b. (At times between 0 and ≈ 12, g decays.) The finite element calculation confirms the expectation that when the decay ceases, the terms in the third-order perturbation analysis with wave number $k_3 + k_2 - k_1 = 3/10$ give 2 turning points to the graph of r versus x (for $0 \leq x < 20\pi/3$). The terms in the fifth-order perturbation analysis with wave number $3k_2 - 2k_1 = 6/10$ give 4 turning points to r versus x at the times for which such graphs are shown in Fig. 5c. As we see in Fig. 5d, the 4 turning points remain present until $t = t^*$.

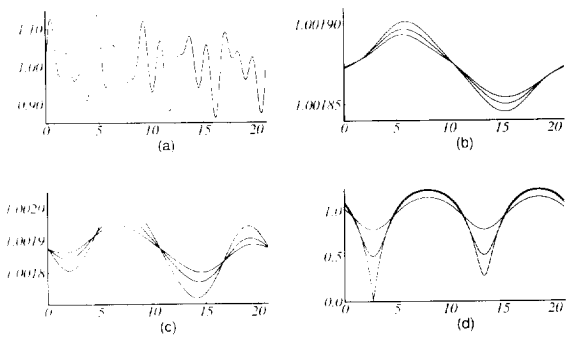

Fig. 5. The radius r as a function of x at various t with $r_0(x)$ as in Eq. (59): (a) $t = 0$ ($g = 0.1393$); (b) $t = 12$ ($g = 2.07 \times 10^{-5}$), $t = 14$ ($g = 2.49 \times 10^{-5}$), $t = 16$ ($g = 2.97 \times 10^{-5}$); (c) $t = 25$ ($g = 7.58 \times 10^{-5}$), $t = 27.5$ ($g = 1.06 \times 10^{-4}$), $t = 30$ ($g = 1.55 \times 10^{-4}$); (d) $t = 62.5$ ($g = 0.2107$), $t = 64.5$ ($g = 0.5027$), $t = t^* = 64.7862$.

Calculated profiles of the body for selected times between $t = 0$ and t^* are shown in Fig. 6. The range of x is again $0 \leq x < 20\pi/3$. The initial profile is seen in Fig. 6a. For each t for which results are shown in Figs. 5 and 6, the corresponding value of g is given in the figure caption. If we again set $\nu = 0.05$, then we here have $t_\# \approx 57$, and the incubation time $t_\#$ is about 88% of the break-up time t^*.

In this numerical experiment, the break-up at $t = t^*$ again results in subbodies that are congruent and star shaped. In Fig. 6f, which shows the profile at time t^*, we see that r has a local minimum with $r > 0$ at $x_{\min,\mathrm{loc}} = x^* + 10\pi/3$. Using the point $(x, r) = (x_{\min,\mathrm{loc}}, 0)$ as the origin of a spherical coordinate system (with the x-axis again the polar axis) we followed the evolution

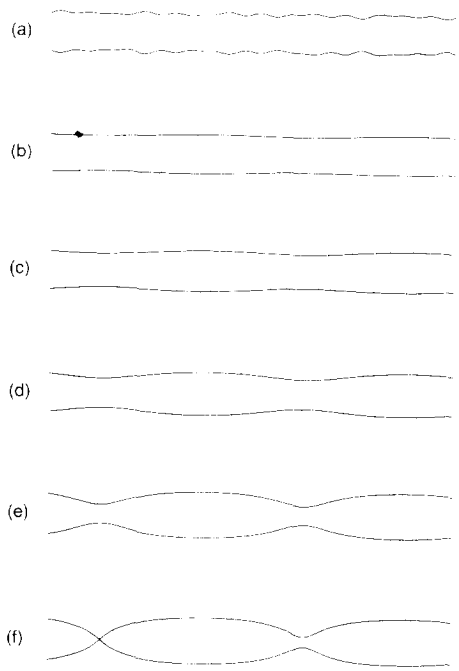

Fig. 6. Configurations attained at selected times before the first break-up implied by the initial data of Eq. (59): (a) $t = 0$ ($g = 0.1393$); (b) $t = 57$ ($g = 0.0481$); (c) $t = 60$ ($g = 0.1035$); (d) $t = 62.5$ ($g = 0.2107$); (e) $t = 64.5$ ($g = 0.5027$); (f) $t = t^* = 64.7862$.

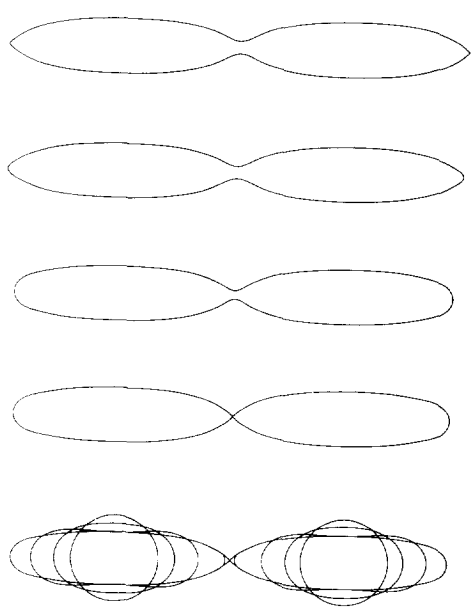

Fig. 7. Configurations attained at times after the time t^* of the first break-up implied by the initial data of Eq. (59). From the top down: $t = t^* + \hat{t}$ with $\hat{t} = 0$, 10^{-4}, 2×10^{-2}, 2.724×10^{-2}. At the bottom are shown configurations at times $t = t^{**} + \bar{t}$ with $\bar{t} = 0$, 10^{-3}, 5×10^{-1}, 2, 8.

of a subbody for $t > t^*$ until a second time of break-up, t^{**}. The results are shown in Fig. 7, where the range of x is from $x_1^* = 2.74071$ to $x_2^* = x_1^* + 20\pi/3$. At time $t = t^{**} = t^* + 0.02724$, the subbody formed at $t = t^*$ breaks into two congruent subbodies. The evolution of these two subbodies was followed for $t > t^{**}$ by re-parameterizing the surface of each using a spherical coordinate system with origin on the x-axis at (dimensionless) distance 5 from the nearest point such that $(x, r) = (x^{**}, 0)$ with x^{**} obeying $r(x^{**}, t^{**}) = 0$. The results obtained this way for $t > t^{**}$, seen at the bottom in Fig. 7, show that the closed surfaces formed at $t = t^{**}$ evolve to form spheres after losing and regaining the convexity they have at $t^{**}+$. We found that at the time $t = t^{**} + 8$ each of these closed surfaces is close to a sphere in the sense that $H/2$ at each of the 401 mesh points employed in its discretization equals, to within 6 significant figures, $(4\pi/3V)^{1/3}$ with V its volume. Thus, in this case, the final equilibrium state of the body with the profile seen in Fig. 6a is an infinite collection of separated spheres, each of which has volume

$$V = (P/M)\langle v \rangle , \tag{61}$$

where $\langle v \rangle$ is as in Eqs. (21) and (23), $P = 20\pi/3$ is the minimum period of u, and $M = 2$ is the number of congruent subbodies formed in an interval of length P at the final break-up time t^{**}.

In the two numerical experiments we have discussed here, the final break-up resulting from a perturbation with the periods P_i in Eq. (5) commensurate gives rise to congruent subbodies. (The volume of the spheres forming the equilibrium state attained at the end of the first numerical experiment is given by Eq. (61) with $P = 4\pi$ and $M = 1$ the number of congruent bodies formed in an interval of length P at time t^*.) However, it is not difficult to show that there is *not* a general rule to the effect that when the

periods P_i in Eq. (5) are both commensurate and such that the final equilibrium state of the perturbed cylinder is a necklace of separated spheres, these spheres are congruent. Examples of perturbations evolving into equilibrium states made up of spheres not all congruent will be discussed in a subsequent paper.

Acknowledgements

We are grateful to Michael Grinfeld, Armen G. Khatchaturyan, and Victor J. Mizel for valuable discussions. This research was supported by the National Science Foundation under Grants DMS-94-04580 and DMS-94-03552, and by the Donors of the Petroleum Research Fund, administered by the American Chemical Society.

References

[1] C. Herring, Surface diffusion as a motivation for sintering, in: The Physics of Powder Metallurgy, W.E. Kingston, ed. (McGraw Hill, New York, 1951) pp. 143–179.

[2] W.W. Mullins, Theory of thermal grooving, J. Appl. Phys. 28 (1957) 333–339.

[3] F.A. Nichols and W.W. Mullins, Surface- (interface-) and volume-diffusion contributions to morphological changes driven by capillarity, Trans. Metall. Soc., AIME 233 (1965) 1840–1847.

[4] C. Corduneanu, Almost Periodic Functions (Interscience, New York, 1968).

[5] A.M. Fink, Almost periodic differential equations, Springer Lecture Notes in Mathematics, No. 377 (Springer, Berlin, 1974) pp. 36–76.

[6] B.D. Coleman, R.S. Falk and M. Moakher, Space–time finite element methods for surface diffusion with applications to the stability of cylinders, SIAM J. Sci. Comp., in press.

[7] T.F. Marinis and R.F. Sekerka, A model for capillary induced instabilties in directionally solidified eutectic alloys, in: Proc. Conf. on *In situ* composites – III, Materials Research Soceity, J.L. Walter, M.F. Gigliotti, B.F. Oliver and H. Bibring, eds. (Ginn Custom, Lexington, 1979) pp. 86–94.

[8] R.F. Sekerka and T.F. Marinis, Dynamics of morphological change during solid–solid transformations, in: Proc. Int. Conf. on Solid–Solid Phase Transformations (AIME, New York, 1983) pp. 67–84.

[9] J.K. Lee and T.H. Courtney, Two-dimensional finite difference analysis of shape instabilities in plates, Metall. Trans. 20 A (1989) 1385–1394.

[10] J.C. Malzahn Kampe, T.H. Courtney and Y. Leng, Shape instabilities of plate-like structures – I. Experimental observations in heavily cold worked *in situ* composites, Acta Metall. 37 (1989) 1735–1745.

[11] G. Huisken, Flow by mean curvature of convex surfaces into spheres, J. Diff. Geom. 20 (1984) 237–266.